

# Nodeless pairing in superconducting copper-oxide monolayer films on $\text{Bi}_2\text{Sr}_2\text{CaCu}_2\text{O}_{8+\delta}$

Yong Zhong<sup>1†</sup>, Yang Wang<sup>1†</sup>, Sha Han<sup>1</sup>, Yan-Feng Lv<sup>1</sup>, Wen-Lin Wang<sup>1</sup>, Ding Zhang<sup>1</sup>, Hao Ding<sup>1</sup>,  
Yi-Min Zhang<sup>1</sup>, Lili Wang<sup>1,2</sup>, Ke He<sup>1,2</sup>, Ruidan Zhong<sup>3,4</sup>, John A. Schneeloch<sup>3,4</sup>, Gen-Da Gu<sup>3</sup>,  
Can-Li Song<sup>1,2\*\*</sup>, Xu-Cun Ma<sup>1,2\*\*</sup>, and Qi-Kun Xue<sup>1,2\*\*</sup>

1 State Key Laboratory of Low-Dimensional Quantum Physics, Department of Physics,  
Tsinghua University, Beijing 100084, China

2 Collaborative Innovation Center of Quantum Matter, Beijing 100084, China

3 Condensed Matter Physics and Materials Science Department, Brookhaven National Laboratory,  
Upton, NY 11973, USA

4 Department of Physics & Astronomy, Stony Brook University, Stony Brook, NY 11794, USA

\*\*To whom correspondence should be addressed. Email: clsong07@mail.tsinghua.edu.cn,  
xucunma@mail.tsinghua.edu.cn, qkxue@mail.tsinghua.edu.cn

†Authors equally contributed to this work.

**Abstract** The pairing mechanism of high-temperature superconductivity in cuprates remains the biggest unresolved mystery in condensed matter physics. To solve the problem, one of the most effective approaches is to investigate directly the superconducting  $\text{CuO}_2$  layers. Here, by growing  $\text{CuO}_2$  monolayer films on  $\text{Bi}_2\text{Sr}_2\text{CaCu}_2\text{O}_{8+\delta}$  substrates, we identify two distinct and spatially separated energy gaps centered at the Fermi energy, a smaller U-like gap and a larger V-like gap on the films, and study their interactions with alien atoms by low-temperature scanning tunneling microscopy. The newly discovered U-like gap exhibits strong phase coherence and is immune to scattering by K, Cs and Ag atoms, suggesting its nature as a nodeless superconducting gap in the  $\text{CuO}_2$  layers, whereas the V-like gap agrees with the well-known pseudogap state in the underdoped regime. Our results support an *s*-wave superconductivity in  $\text{Bi}_2\text{Sr}_2\text{CaCu}_2\text{O}_{8+\delta}$ , which, we propose, originates from the modulation-doping resultant two-dimensional hole liquid confined in the  $\text{CuO}_2$  layers.

**Keywords:** Copper oxides · Molecular beam epitaxy · Nodeless pairing · Modulation doping

## 1 Introduction

The discovery of high temperature ( $T_c$ ) superconductivity (HTS) in cuprates [1] has triggered tremendous efforts to elucidate as to why they superconduct at high  $T_c$ . However, this enigma remains unresolved, apparently owing to the layered structure in which the superconducting  $\text{CuO}_2$  layers are sandwiched between non-superconducting charge reservoir layers, for example,  $\text{BiO/SrO}$  in the case of  $\text{Bi}_2\text{Sr}_2\text{CaCu}_2\text{O}_{8+\delta}$  (Bi-2212). Upon chemical doping in the reservoir layers, rather than direct chemical doping in the  $\text{CuO}_2$  layers, the resulting carriers transfer into the  $\text{CuO}_2$  layers and boost superconductivity therein, resembling the HTS in single-unit-cell FeSe films on  $\text{SrTiO}_3$  [2]. By layer-by-layer removal with an  $\text{Ar}^+$  bombardment technique, we could reveal respective quasiparticle (QP) excitations of the constituent planes of Bi-2212 [3] and Bi-2201 [4]. However, the  $\text{CuO}_2$  surface obtained is too small to systematically investigate its superconducting property.

Here we grow ultrathin  $\text{CuO}_2$  films on the  $\text{BiO}$  surfaces of the cleaved Bi-2212 crystals by a state-of-the-art ozone molecular beam epitaxy (MBE) technique. This approach allows direct measurements of the electronic structure of the  $\text{CuO}_2$  layers by *in situ* scanning tunneling microscopy (STM). We demonstrate that the superconducting gap in the  $\text{CuO}_2$  layers is nodeless, contradictory to the nodal  $d$ -wave pairing scenario that is often thought to be the most important result in the thirty-year study of the HTS mechanism of cuprates.

## 2 Experimental

Our experiments were conducted in an ultrahigh vacuum low temperature STM system equipped with ozone-assisted MBE chamber (Unisoku), with a base pressure of  $\sim 1 \times 10^{-10}$  Torr. The

copper-oxide films were prepared by evaporating high-purity Cu (99.9999%) sources from a standard Knudsen cell under ozone flux beam of  $1.0 \sim 5.0 \times 10^{-5}$  Torr. The flux beam of ozone from a home-built ozone gas delivery system was injected into the MBE using a 1/2 inch stainless tube (Swagelok),  $\sim 50$  mm distant from the sample. The K, Cs and Ag atoms were respectively evaporated from alkali-metal dispensers (SAES Getters) and home-made Ta boat, with the samples kept at approximately 50 K. Polycrystalline PtIr tips were cleaned by *e*-beam heating in UHV and calibrated on the MBE-grown Ag/Si(111) films before STM measurements. All STM images were acquired at 4.2 K in constant-current mode, and the differential tunneling  $dI/dV$  spectra were measured by using a standard lock-in technique with a small bias modulation of 1 mV at 966 Hz, unless otherwise specified.

### 3 Results and discussion

MBE growth of copper-oxide films on Bi-2212 with  $T_c = 91$  K (Fig. 1a-d) proceeds in layer-by-layer mode, and epitaxial crystalline films down to a single monolayer (ML) could be prepared. The STM topographic images (Fig. 1a, d) reveal atomically flat and nearly defect-free surfaces on the cleaved Bi-2212 crystal. The characteristic *b*-axis supermodulation (Fig. 1c) is clearly seen in the uncovered BiO regions in Fig. 1a. The atomically resolved image in Fig. 1d reveals the nearest-neighbor Cu ions in the monolayer films to be  $3.8 \text{ \AA}$  apart. The square structure and the in-plane lattice constant are consistent with those of the  $\text{CuO}_2$  plane in bulk Bi-2212. For rocksalt-structured tetragonal CuO (T-CuO) [5-7], a  $\sqrt{2} \times \sqrt{2}$  surface reconstruction might blur half Cu ions and lead to the same lattice constant. However, the identification of the films as  $\text{CuO}_2$  is sustained by a large separation of 2.35 eV between the Fermi level ( $E_F$ ) and the valence band of T-CuO [6], while the corresponding value here is only 1.40 eV (Fig. 1e).

In scanning tunneling spectroscopy (STS), the differential conductance  $dI/dV$  measures the local density of states (DOS) as a function of bias voltage ( $V$ ). Our  $dI/dV$  measurements reveal several distinctive features of the  $\text{CuO}_2$  films from the cleaved  $\text{BiO}$  surfaces that have been extensively studied by STM/STS [8]. First, the overall electronic spectrum of the  $\text{CuO}_2$  films is characterized by a Mott-Hubbard-like gap of 2.21 eV without prominent states in it (Fig. 1e). The result is expected since the ground state of  $\text{CuO}_2$  is a Mott insulator as previously observed by STM in  $\text{Ca}_2\text{CuO}_2\text{Cl}_2$  [9]. The pronounced DOS at 1.1 eV can be assigned to the upper Hubbard band, while the shoulders around -1.82 eV (see the arrow in Fig. 1e) the charge transfer band (CTB) [10] or Zhang-Rice-Singlet [11] because of strong on-site Coulomb repulsion. The CTB gap magnitude of 2.21 eV agrees with 2.2 eV as measured in  $\text{Ca}_2\text{CuO}_2\text{Cl}_2$  [9] and 2.0 eV for  $\text{La}_{2-x}\text{Sr}_x\text{Cu}_2\text{O}_4$  [12].

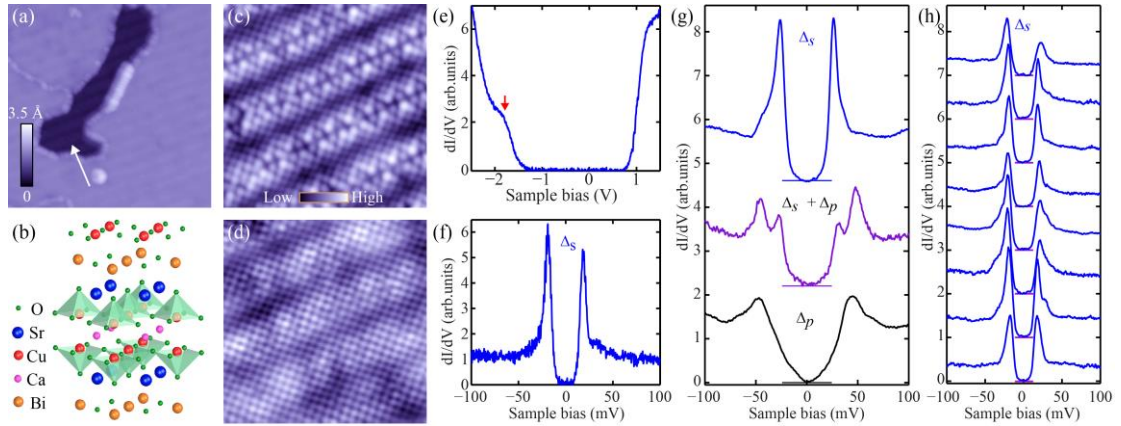


**Fig. 1.** STM characterization of  $\text{CuO}_2$  monolayer films on Bi-2212. **a, b** STM topography ( $V = 1.5$  V,  $I = 20$  pA,  $40$  nm  $\times$   $40$  nm) and schematic view of monolayer  $\text{CuO}_2$  films on the Bi-2212 substrate. The arrow indicates the uncovered  $\text{BiO}$  surface. **c** STM topography ( $V = 0.2$  V,  $I = 50$  pA,  $10$  nm  $\times$   $10$  nm) on the  $\text{BiO}$  surface. **d** STM topography ( $V = 0.5$  V,  $I = 15$  pA,  $10$  nm  $\times$   $10$  nm) of the  $\text{CuO}_2$  films showing a square lattice with Cu-Cu spacing of  $3.8$  Å. **e** Large-energy-scale  $dI/dV$  spectrum (setpoint:  $V = 1.5$  V,  $I = 100$  pA) on  $\text{CuO}_2$ . The bias-modulation amplitude was set to  $15$  mV<sub>rms</sub>. **f, g**  $dI/dV$  spectra of the  $\text{CuO}_2$  films, revealing two distinct energy scale gaps ( $\Delta_s$  and  $\Delta_p$ ) in the low-energy QP excitations. The U-shaped spectra exhibit vanishing and particle-hole-symmetric

DOS over a finite energy range near  $E_F$ . The spectra in (g) were acquired in the same sample and vertically offset for clarity, with their zero-conductance positions marked by the correspondingly colored horizontal lines throughout. **h** Line-cut  $dI/dV$  spectra showing the spatial robustness of the U-shaped superconducting gap in the  $\text{CuO}_2$  films. The eight  $dI/dV$  spectra along 6-nm trajectories on  $\text{CuO}_2$  all show vanishing and particle-hole-symmetric DOS over a finite energy range near  $E_F$ . The purple horizontal bars mark the zero-conductance positions. Setpoint: **f, h**  $V = 0.2$  V,  $I = 100$  pA; **g**  $V = 0.1$  V,  $I = 300$  pA.

Second, and the most surprisingly, in some regions the low-energy QP excitations of the  $\text{CuO}_2$  films disclose a well-defined U-gap (Fig. 1f) ( $\Delta_s$ ). Its two pronounced conductance peaks at gap edges ( $\pm 18.6$  meV) and the vanishing DOS in between, suggest that  $\Delta_s$  is an *s*-wave-like gap. To avoid possible artificial effects in our measurements, we collected more than 3000 spectra on different locations of the  $\text{CuO}_2$  films from more than forty samples. The persistence of the U-gap in these regions is illustrated in Fig. 1h: despite changes in the coherence peak intensity and the gap size ranging from 16 meV to 22 meV, the essential U shape can clearly be seen. The observation invalidates the general assumption that the V-shaped STS spectra on the cleaved BiO surfaces are due to tunneling from the underlying  $\text{CuO}_2$  planes in Bi-2212 [8]. Other regions are characterized by a larger V-shaped gap ( $\Delta_p$ ) (the black curve in Fig. 1g). At boundaries between the two types of regions, a double-gap feature with mixed U- and V-gaps (violet curve in Fig. 1g) is present and expected. Within our instrumental resolution, we find no difference in the detailed features of these V-gaps and the pseudogap (PG) from the BiO surfaces in Fig. 1c [8]. The two-gap feature, together with the systematic spatial evolution of  $dI/dV$  spectra observed throughout, suggests two types of QP gaps at different energy scales in the  $\text{CuO}_2$  films on Bi-2212, although their spectral weights ( $W$ ) are spatially varied. Such spatial inhomogeneity might originate from different amount of charge transfer from the substrate to  $\text{CuO}_2$ , e.g. the U-gap

regions have more hole carriers as compared to the V-gap regions. This charge transfer seems not induce apparent large-energy-scale states in the CTB gap (Fig. 1e). The result is very significant and implies that external doping of the CuO<sub>2</sub> Mott insulator doesn't alter its fundamental electronic structure, an issue fiercely debated but at the heart of HTS physics. It actually forms a starting point of our new model for HTS, as will be discussed later.

What might be the origin of the two-energy-scale QP gaps in the CuO<sub>2</sub> films? To address this issue, in Fig. 2a, we summarize our measurements of the averaged gap magnitudes,  $\Delta_s$  and  $\Delta_p$ , as a function of  $\Delta_{p, \text{BiO}}$  simultaneously acquired on the exposed BiO surfaces. Here  $\Delta_{p, \text{BiO}}$  and thus the hole carriers are delicately controlled by annealing the samples under ozone flux or UHV [3, 4]. The larger energy gap,  $\Delta_p$ , is found to scale linearly with  $\Delta_{p, \text{BiO}}$  and bears striking quantitative correspondence in the magnitude (red dashes) and spatial variation (marked by the equal statistical uncertainty) to  $\Delta_{p, \text{BiO}}$ , further stressing its nature as the gap in Bi-2212 substrates [13]. Therefore, the CuO<sub>2</sub> films in these regions remain at their insulating state and thus transparent to the STM tip. On the other hand, the magnitude of the smaller but relatively homogeneous gap  $\Delta_s$  (documented by the small statistical uncertainty in Fig. 2a) exhibits a different behavior versus  $\Delta_{p, \text{BiO}}$  and saturates at  $\sim 30$  meV. This hints at a different origin of  $\Delta_s$ . As a superconducting gap in the CuO<sub>2</sub> layers, it was occasionally seen in the form of broad 'kinks' in underdoped Bi-2212 [14, 15]. The above results including those from Fig. 1f, g, i, consistently suggest that the U-gap corresponds to a superconductivity state prompted by the charge transfer mentioned above. Because of asymmetric doping and a peculiar bonding configuration of CuO<sub>2</sub> on the inert BiO surface, we speculate that the total charge transfer is not sufficient to make the whole films superconducting, leading to the formation of two different regions. The situation may be improved by growing

CuO<sub>2</sub> on the SrO surface of Bi-2212 [3, 4].

To further confirm that the U-gap regions are superconducting, we investigate the temperature evolution of the  $dI/dV$  spectra (see Fig. 2b, c). The U-gap  $\Delta_s$  exhibits the characteristics of a conventional superconducting gap: with increasing temperature, the coherence peaks begin to fade away abruptly and then gradually (Fig. 2b). At 101 K, the gap vanishes completely. Meanwhile, the DOS near  $E_F$  shows a dramatic increase for  $\Delta_s$ , particularly around 101 K. The results demonstrate that  $\Delta_s$  is indeed a superconducting gap, and that the CuO<sub>2</sub> monolayers on BiO surface are superconducting with  $s$ -wave-like pairing wavefunction. As for  $\Delta_p$ , it is still visible at 104 K and exhibits the same behavior as the PG observed on the cleaved Bi-2212 surfaces [8].

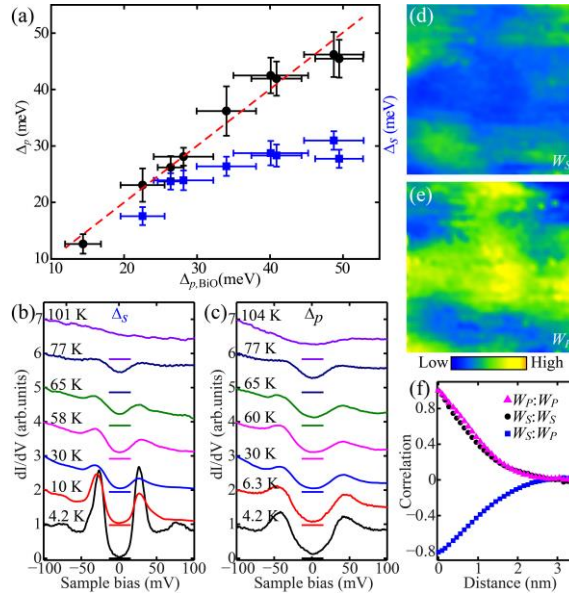


**Fig. 2.** Low-energy QP excitations at two energy scales. **a** Dependence of  $\Delta_s$  (blue squares) and  $\Delta_p$  (black circles) on  $\Delta_{p,BiO}$ . The red diagonal dashes show the curve for  $\Delta_p = \Delta_{p,BiO}$ . The error bars refer to the standard deviation of statistical gap values from 50  $dI/dV$  spectra. **b, c** Temperature dependence of the superconducting gap  $\Delta_s$  and PG  $\Delta_p$ . Distinct from a gradual DOS filling for  $\Delta_p$ , the DOS near  $E_F$  for  $\Delta_s$  shows a more dramatic increase with temperature. Setpoint:  $V = 0.1$  V,  $I = 100$  pA. **d, e** Local DOS images (6 nm  $\times$  6 nm) of  $dI/dV$  spectra measured at

(d)  $V = -25$  mV and (e)  $V = -45$  mV, characterizing the spatial distribution of  $W_{s(p)}$  for the pairing gap  $\Delta_s$  and pseudogap  $\Delta_p$ , respectively. Setpoint:  $V = 50$  mV,  $I = 100$  pA. f Azimuthally averaged autocorrelation of  $W_{s(p)}$  (black circles and magenta triangles) and cross correlation between them (blue squares).

In search for the origin of the nodeless superconductivity observed here, we study the related spectral weight of  $\Delta_{s(p)}$ ,  $W_{s(p)}$ , in the  $\text{CuO}_2$  films. Such  $W_{s(p)}$  images, represented approximately by the  $dI/dV$  conductance at the energies of  $\Delta_s \sim 25$  meV and  $\Delta_p \sim 45$  meV, are simultaneously mapped and shown in Fig. 2d, e. The spatial inhomogeneity in  $W_{s(p)}$  and their anticorrelation are discernable. To quantify this, we compute the cross correlation between  $W_s$  and  $W_p$ , as depicted by blue squares in Fig. 2f. Combined with the  $W_{s(p)}$  autocorrelation (black circles and magenta triangles), we estimate a characteristic correlation length of  $\sim 2.7$  nm over which the correlation goes to zero. The findings are reminiscent of the electronic inhomogeneity with a similar length scale in cuprates [16, 17], which is most likely correlated with interstitial oxygen dopants [17]. The anticorrelation coefficient of -0.8 between  $W_s$  and  $W_p$  is actually quite large, suggesting that the Bi-2212 substrate plays an important role in the observed superconductivity as a charge reservoir. Evidently, the superconducting gap  $\Delta_s$  goes hand in hand with  $\Delta_{p, \text{BiO}}$  (Fig. 2a), an indicator of mobile hole carriers available in the Bi-2212 [18]. Here the anticorrelated  $\Delta_p$  and  $\Delta_s$ , supporting the proposal that the PG in cuprates is competitive with and thus irrelevant to pairing [3, 4, 19, 20], might be only a phenomenological reflection of the available hole carriers for PG formation and Cooper pairing.

Response of the gaps against nonmagnetic impurities further helps unravel the pairing symmetry. Nonmagnetic impurities have been known to exert little or no effect on electron pairing in a conventional  $s$ -wave superconductor [21], but to induce QP bound states within the pairing gap in an unconventional superconductor with gap nodes [22]. To gain insight into  $\Delta_p$  and  $\Delta_s$ , we

deposit alkali-metals (K and Cs) and a noble-metal (Ag) on Bi-2212 and CuO<sub>2</sub> films (see Fig. 3). We find that the PG on Bi-2212 broadens gradually in its magnitude with increasing K (Cs) coverage and vanishes at a K dose of  $\sim 0.168$  ML (Fig. 3g), whereas it changes little on the K, Cs and Ag covered CuO<sub>2</sub> surface (Fig. 3k, n, q). This nicely echoes our argument that the PG is from the substrate: K (Cs) may donate some electrons to the CuO<sub>2</sub> surface [23, 24], but it is limited to the CuO<sub>2</sub> layers (Fig. 3a-f) and shouldn't disturb the substrate electronic structure much. No bound state is seen atop Ag adatoms on the Bi-2212 surface (Fig. 3h), implying that the *d*-wave PG is not a pairing gap, which should otherwise induce in-gap bound states [22]. Importantly, the long hidden superconducting gap  $\Delta_s$  for CuO<sub>2</sub> shows striking robustness against scattering by K, Cs (Fig. 3a, b, d, e), and Ag (Fig. 3g, h) for a wide range of coverage from 0 to 0.84 ML. The results are in line with the nodeless *s*-wave pairing and against sign-reversal pairing symmetry.

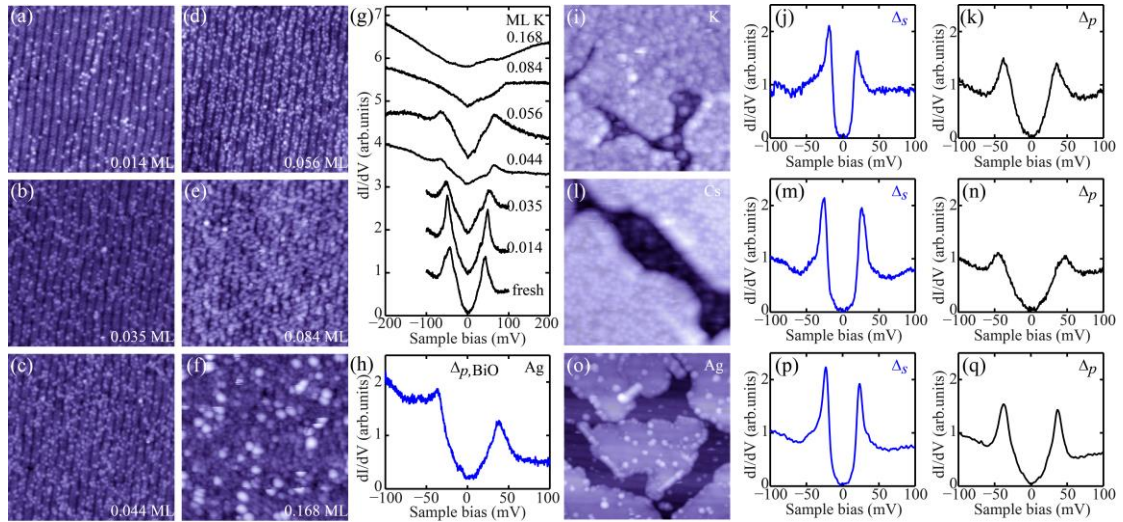


**Fig. 3.** Immunity of QP energy gaps to non-magnetic impurities. **a-f** STM topography ( $V = 0.4$  V,  $I = 20$  pA,  $50$  nm  $\times$   $50$  nm) of the cleaved Bi-2212 surface adsorbed with K at different dosages, as indicated. Here 1 ML is defined as the areal density of Bi at the topmost BiO layer ( $\sim 6.9 \times 10^{14}/\text{cm}^2$ ). **g** K coverage-dependent  $dI/dV$  spectra on the cleaved Bi-2212 surface at 4.2 K. Setpoint:  $I = 200$  pA and  $V = 0.1$  V (the three curves from the bottom) or 0.2 V (the upper four curves). **h** Typical  $dI/dV$  spectrum (setpoint:  $V = 0.2$  V,  $I = 200$  pA) measured on Ag adatoms on Bi-2212, revealing no in-gap states within the pseudogap. **i-k** STM topography ( $V = 1.2$  V,  $I = 10$  pA,  $50$  nm  $\times$   $50$

nm) and  $dI/dV$  spectra (setpoint:  $V = 0.2$  V,  $I = 200$  pA) of  $\sim 0.84$  ML K-dosed  $\text{CuO}_2$  monolayer films. **l-n** STM topography ( $V = 1.5$  V,  $I = 10$  pA,  $30$  nm  $\times$   $30$  nm) and  $dI/dV$  spectra (setpoint:  $V = 0.2$  V,  $I = 200$  pA) of  $\sim 0.03$  ML Cs-dosed  $\text{CuO}_2$  monolayer films. **o-q** STM topography ( $V = 1.2$  V,  $I = 20$  pA,  $50$  nm  $\times$   $50$  nm) and  $dI/dV$  spectra (setpoint:  $V = 0.2$  V,  $I = 200$  pA) of Ag-dosed  $\text{CuO}_2$  monolayer films. The spectra were measured on K, Cs or Ag adatoms, revealing undisturbed energy gaps against nonmagnetic impurity scattering.

One may argue that lifting of gap nodes by disorder might engender a U-shaped gap structure. For hypothesized  $d$ -wave pairing in cuprates, the positions and topology of nodes are rigorously imposed by the symmetry, and thus the gapless excitations are protected against disorder. In this case, the disorder would have severely suppressed the coherence peaks, contradicting our observations (Fig. 1f, g, i). One may also argue that the U-gap results from the anisotropic tunneling matrix element  $T_\phi \propto \cos^2 2\phi$  ( $\phi = \tan^{-1}(k_y/k_x)$  is the azimuthal tunneling angle) effects for  $\text{CuO}_2$  with tetragonal symmetry [25]. Such a  $T_\phi$  reduces the low-energy QP tunneling in the nodal regions of  $d$ -wave gap and can give rise to a U-like spectrum, while sharpening the coherence peaks. We have attempted the method to fit our data, but no success (Fig. 4), which suggests that  $\Delta_s$  is isotropic in reciprocal space. Further theoretical study is needed to understand how the pairing is intertwined with PG [26] and the resultant U-like excitations in  $\text{CuO}_2$ .

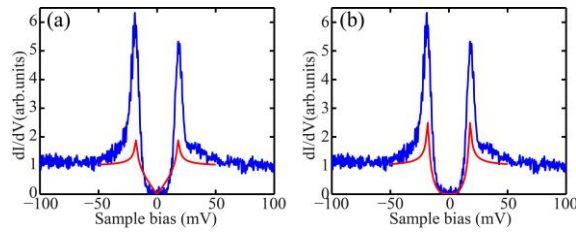


**Fig. 4.** Fits (red curve) of the U-like  $dI/dV$  spectrum of Fig. 1f (blue curve) to (a) a standard  $d$ -wave and (b)  $T_\phi$ -filtered  $d$ -wave. The experimental spectrum shows remarkably strong coherence peaks and cannot be reconciled with a  $d$ -wave gap even after an inclusion of the anisotropic matrix effects. An instrumental broadening parameter  $\Gamma = 0.1$  meV is used for the fits.

Our results on the nodeless gap of the superconducting  $\text{CuO}_2$  monolayers, which is evidently

triggered by charge transfer from the substrate, have significant implications on the pairing mechanism of Bi-2212. The undoped  $\text{CuO}_2$  is well known as a Mott insulator due to many-body correlation. It becomes superconducting only when the adjacent BiO/SrO reservoir layers are doped and the resulting carriers are injected into it. Such charge-transfer mechanism has long been employed as modulation-doping in semiconductor high-electron-mobility-transistors such as  $\text{Al}_x\text{Ga}_{1-x}\text{As}/\text{GaAs}$  superlattices [27], as schematically illustrated in Fig. 5a. It is well-established that charge transfer is initiated only when the  $E_F$  of doped n-type  $\text{Al}_x\text{Ga}_{1-x}\text{As}$  is higher than that of undoped GaAs. Upon contact, charge transfer and band bending take place to align their Fermi levels, which, in turn, leads to formation of a quantum well (QW) at the GaAs side of the interface. The transferred carriers form a two-dimensional electron gas (2DEG) in the QW, while  $\text{Al}_x\text{Ga}_{1-x}\text{As}$  is depleted forming a potential barrier. Without band bending and QW formation, GaAs itself is insulating and cannot accommodate electrons. Similarly, the holes cannot be injected into the  $\text{CuO}_2$  Mott insulator unless a QW forms in the  $\text{CuO}_2$  layer (Fig. 5b). As a result, the hole carriers generated in the SrO(BiO) layers “fall” into the  $\text{CuO}_2$  QW and form a clean 2D hole liquid (2DHL) therein. Formation of 2DHL does not necessarily change the ground electronic state of  $\text{CuO}_2$ , as in the case of  $\text{Al}_x\text{Ga}_{1-x}\text{As}/\text{GaAs}$  in the spirit of rigid-band model. This argument is supported by our observations in Fig. 1e, and also by resonant inelastic X-ray scattering study showing the persistence of anti-ferromagnetic ordering in  $\text{CuO}_2$  for the whole phase diagram of  $\text{La}_{2-x}\text{Sr}_x\text{Cu}_2\text{O}_4$  ( $x = 0$  to 0.40) [28]. In this way, regardless of how much the doping is, the  $\text{CuO}_2$  planes can sustain its chemical and structural integrity so as to assure the superconductivity phase coherence. Under this context, Bi-2212 is nothing special but just a 2DHL superlattice with much higher carrier density. The 2DHL confined in the  $\text{CuO}_2$  layers should have a simple concentric circular

Fermi surface, which may naturally lead to an isotropic pairing and a conventional  $s$ -wave gap. Indeed, the single-unit-cell FeSe films on SrTiO<sub>3</sub> are found to exhibit a simple Fermi surface and conventional  $s$ -wave superconductivity [2, 29], which result from the same charge transfer mechanism.

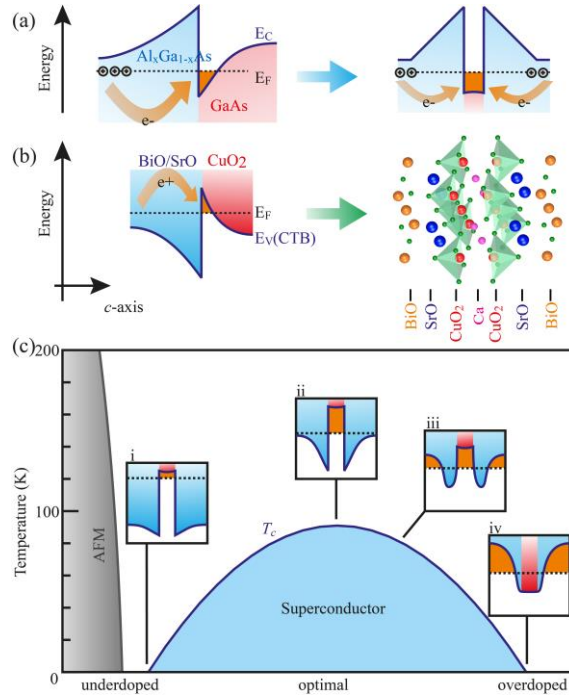


**Fig. 5.** Modulation doping scheme and superconductivity in cuprates. **a, b** Energy-band diagram and formation of quantum wells for  $\text{Al}_x\text{Ga}_{1-x}\text{As}/\text{GaAs}$  and  $\text{SrO}(\text{BiO})/\text{CuO}_2$  heterostructures, respectively. Mobile electrons or holes are transferred from the modulation doping layers to either the interface or the quantum wells (indicated by the orange arrows). **c** Phase diagram of high- $T_c$  cuprate superconductors, interpreted as the evolution of a quantum well under modulation doping of holes.

We now show that with this rather simple model, we can understand the complicated phase diagram of cuprates [30]. As schematically illustrated in Fig. 5c, at critical doping the superconductivity sets in as the  $\text{CuO}_2$  QW is filled with sufficient holes to form 2DHL (panel i in Fig. 5c). Increasing doping concentration pulls down the  $E_F$  of the reservoir layers such that the hole density in the QW increases (so does  $T_c$ ). The optimal doping corresponds to the situation

where the QW reaches its maximal capacity to accommodate holes (panel ii in Fig. 5c). Further doping into the reservoir layers results in a parallel conductive channel and the  $\text{CuO}_2$  QW starts to collapse (panel iii in Fig. 5c), which reduces the effective hole density in the  $\text{CuO}_2$  layer and thus weakens the superconductivity. In the extremely overdoped regime where the  $E_F$  touches the CTB of  $\text{CuO}_2$  (panel iv in Fig. 5c), the charge transfer no longer exists. As a result, the QW is not filled and the  $\text{CuO}_2$  layer returns to its initial insulating state, while the reservoir layers become highly conductive. Note that the charge carriers generated in the reservoir layers increase monotonically with chemical doping (Fig. 5c). It is consistent with the linear reduction of  $\Delta_p$  with increasing doping and supports the origin of PG from the reservoir layers.

The strange metal phase around the overdoped regime is regarded as one of the most mysterious puzzles in cuprates [30]. According to our model, the Bi-2212 in this regime (panel iii in Fig. 5c) is composed of alternative 2DHL layers and SrO/BiO reservoir layers that are both conducting. Unlike a conventional metal, the carrier density of these layers can be thermally activated, just like doped semiconductors. This fact would complicate the resistivity versus temperature behavior, and the peculiar linearly temperature-dependent resistivity in cuprates results simply from the intertwined effects of a quadratic scattering rate (Fermi liquid behavior) and temperature-dependent carrier density [31]. Moreover, other normal state properties of cuprates in the whole phase diagram can be understood easily: they should also be dominated by complicated behaviors of the heavily doped charge reservoir layers because the  $\text{CuO}_2$  planes contribute little to those behaviors (particularly resistivity) above  $T_c$  because of disappearing hole-dopant ion separation.

For both cuprates and iron-based superconductors, particle-hole-asymmetric

superconductivity domes have been revealed in phase diagrams. We believe that it originates from particle-hole-asymmetric band offsets of different reservoir layers with regard to  $\text{CuO}_2$  that make up the superconductor, because the Fermi level of the undoped charge reservoir layers and the mid-gap position of the Mott insulator  $\text{CuO}_2$  are usually different. In the case that the band offset doesn't allow enough charge transfer, superconductivity dome may not emerge.

Finally, we would like to point out that the monolayer oxide films studied here might be T-CuO, whose ground state is also a Mott insulator and similar to  $\text{CuO}_2$  [6]. As discussed above, whether it is  $\text{CuO}_2$  or T-CuO doesn't affect the modulation-doping scheme: as long as a material can form an ideal heterostructure with it and their respective electronic structures satisfy the criterion for band bending, the system may superconduct. The  $\text{FeSe}/\text{SrTiO}_3$  and  $\text{LaAlO}_3/\text{SrTiO}_3$  heterostructures represent two good examples [2, 32].

#### **4 Summary**

Our model is based on the modulation-doping scheme that is in the framework of rigid band model and has been proved extremely successful in semiconductor physics since its development in late 1970's [27]. Although this rigid-band model based scheme is simple, we have shown that it could capture the essential features of Bi-2212 for both normal and superconducting states in the entire phase diagram. The model may also work for other cuprates and iron-based superconductors in terms of the same doping-charge-transfer mechanism. To justify the model, here we propose to employ electrical field effect (e.g. by ionic liquids) to tune the copper-oxide layers on non-superconducting substrates (such as  $\text{SrTiO}_3(001)$ ) superconducting. If the model is confirmed, it would point to an explicit direction for discovering new high- $T_c$  materials, as has been done for the quantum Hall effect with various semiconductor heterostructures. Last but not least, the

observed nodeless superconductivity implies that the pairing might be mediated by an attractive interaction in  $k$  space, probably associated with electron-phonon interaction as in conventional superconductors. Therefore, exploring the isotope effect of  $T_c$  will help unravel the pairing mechanism. The successful growth of  $\text{CuO}_2$  monolayer films, as reported here, paves a solid base for future study.

**Acknowledgments** The work was financially supported by National Science Foundation, Ministry of Science and Technology and Ministry of Education of China. The work at Brookhaven National Laboratory was supported by the Office of Basic Energy Sciences, U.S. Department of Energy, under Contract No. DE-SC00112704.

**Conflict of interest** The authors declare that they have no conflict of interest.

## References

1. Bednorz JP, Müller KA (1986) Possible high  $T_c$  superconductivity in the Ba-La-Cu-O system. *Z Phys B* 64: 189-193
2. Wang QY, Li Z, Zhang WH et al (2012) Interface-induced high-temperature superconductivity in single unit-cell FeSe films on  $\text{SrTiO}_3$ . *Chin Phys Lett* 29: 037402
3. Lv YF, Wang WL, Peng JP et al (2015) Mapping the electronic structure of each ingredient oxide layer of high- $T_c$  cuprate superconductor  $\text{Bi}_2\text{Sr}_2\text{CaCu}_2\text{O}_{8+\delta}$ . *Phys Rev Lett* 115: 237002
4. Lv YF, Wang WL, Ding H et al (2016) Electronic structure of the ingredient planes of the cuprate superconductor  $\text{Bi}_2\text{Sr}_2\text{CuO}_{6+\delta}$ : a comparison study with  $\text{Bi}_2\text{Sr}_2\text{CaCu}_2\text{O}_{8+\delta}$ . *Phys Rev B* 93: 140504
5. Siemons W, Koster G, Blank DH et al (2009) Tetragonal CuO: End member of the 3d transition metal monoxides. *Phys Rev B* 79: 195122
6. Moser S, Moreschini L, Yang HY et al (2014) Angle-resolved photoemission spectroscopy of tetragonal CuO: Evidence for intralayer coupling between cupratelike sublattices. *Phys Rev Lett* 113: 187001

7. Adolphs CP, Moser S, Sawatzky GA et al (2016) Non-Zhang-Rice singlet character of the first ionization state of T-CuO. *Phys Rev Lett* 116: 087002
8. Fischer Ø, Kugler M, Maggio-Aprile I et al (2007) Scanning tunneling spectroscopy of high-temperature superconductors. *Rev Mod Phys* 79: 353-419
9. Ye C, Cai P, Yu RZ et al (2013) Visualizing the atomic-scale electronic structure of the  $\text{Ca}_2\text{CuO}_2\text{Cl}_2$  Mott insulator. *Nature Commun* 4: 1365
10. Zaanen J, Sawatzky GA, Allen JW (1985) Band gaps and electronic structure of transition-metal compounds. *Phys Rev Lett* 55: 418-421
11. Zhang FC, Rice TM (1988) Effective Hamiltonian for the superconducting Cu oxides. *Phys Rev B* 37: 3759-3761
12. Kastner MA, Birgeneau RJ, Shirane G et al (1998) Magnetic, transport, and optical properties of monolayer copper oxides. *Rev Mod Phys* 70: 897-928
13. Hashimoto M, Vishik IM, He RH et al (2014) Energy gaps in high-transition-temperature cuprate superconductors. *Nature Phys* 10: 483-495
14. Pushp A, Parker CV, Pasupathy AN et al (2009) Extending universal nodal excitations optimizes superconductivity in  $\text{Bi}_2\text{Sr}_2\text{CaCu}_2\text{O}_{8+\delta}$ . *Science* 324: 1689-1693
15. Alldredge JW, Lee J, McElroy K et al (2008) Evolution of the electronic excitation spectrum with strongly diminishing hole density in superconducting  $\text{Bi}_2\text{Sr}_2\text{CaCu}_2\text{O}_{8+\delta}$ . *Nature Phys* 4: 319-326
16. Pan SH, O'Neal JP, Badzey RL et al (2001) Microscopic electronic inhomogeneity in the high- $T_c$  superconductor  $\text{Bi}_2\text{Sr}_2\text{CaCu}_2\text{O}_{8+\delta}$ . *Nature* 413: 282-285
17. McElroy K, Lee J, Slezak JA et al (2005) Atomic-scale sources and mechanism of the nanoscale electronic disorder in  $\text{Bi}_2\text{Sr}_2\text{CaCu}_2\text{O}_{8+\delta}$ . *Science* 309: 1048-1052
18. Huefner S, Hossain MA, Damascelli et al (2008) Two gaps make a high temperature superconductor? *Rep Prog Phys* 71: 062501
19. Kondo T, Khasanov R, Takeuchi T et al (2009) Competition between the pseudogap and superconductivity in the high- $T_c$  copper oxides. *Nature* 457: 296-300
20. Chakravarty S, Laughlin RB, Morr DK et al (2001) Hidden order in the cuprates. *Phys Rev B* 63: 094503

21. Yazdani A, Jones BA, Lutz CP et al (1997) Probing the local effects of magnetic impurities on superconductivity. *Science* 275: 1767-1770
22. Balatsky AV, Vekhter I, Zhu JX (2006) Impurity-induced states in conventional and unconventional superconductors. *Rev Mod Phys* 78: 373-433
23. Kim YK, Krupin O, Denlinger JD et al (2014) Fermi arcs in a doped pseudospin-1/2 Heisenberg antiferromagnet. *Science* 345: 187-190
24. Kim YK, Sung NH, Denlinger JD et al (2016) Observation of a *d*-wave gap in electron-doped Sr<sub>2</sub>IrO<sub>4</sub>. *Nature Phys* 12: 37-41
25. Su YH, Luo HG, Xiang T (2006) Universal scaling behavior of the *c*-axis resistivity of high-temperature superconductors. *Phys Rev B* 73: 134510
26. Mishra V, Chatterjee U, Campuzano JC et al (2014) Effect of the pseudogap on the transition temperature in the cuprates and implications for its origin. *Nature Phys* 10: 357-360
27. Dingle R, Störmer HL, Gossard AC et al (1978) Electron mobilities in modulation-doped semiconductor heterojunction superlattices. *Appl Phys Lett* 33: 665-667
28. Dean MP, Dellea G, Springell RS et al (2013) Persistence of magnetic excitations in La<sub>2-x</sub>Sr<sub>x</sub>CuO<sub>4</sub> from the undoped insulator to the heavily overdoped non-superconducting metal. *Nature Mater* 12: 1019-1023
29. Fan Q, Zhang WH, Liu X et al (2015) Plain *s*-wave superconductivity in single-layer FeSe on SrTiO<sub>3</sub> probed by scanning tunneling microscopy. *Nature Phys* 11: 946-952
30. Keimer B, Kivelson SA, Norman MR et al (2014) From quantum matter to high-temperature superconductivity in copper oxides. *Nature* 518: 179-186
31. Barišić N, Chan MK, Veit MJ et al (2015) Hidden Fermi-liquid behavior throughout the phase diagram of the cuprates. arXiv: 1507.07885
32. Reyren N, Thiel S, Cavaglia AD et al (2007) Superconducting interfaces between insulating oxides. *Science* 317: 1196-1199